Electronic structure of AlAs-GaAs superlattices

M. C. Muñoz, V. R. Velasco, and F. García-Moliner
Instituto de Ciencia de Materiales, Consejo Superior de Investigaciones Científicas (CSIC), Serrano 123, E-28006 Madrid, Spain
(Received 4 August 1988)

The electronic structure of (001) AlAs-GaAs superlattices is studied for $(2,2) \leq (n,m) \leq (22,22)$, where n (m) is the number of principal layers of AlAs (GaAs). Four distinct regions are identified in the (n,m) chart. Only one has an indirect gap. Besides energy eigenvalues, especially band-edge levels, attention is paid to confinement problems and the spatial dependence of the local amplitude of several representative states. The results show a very diversified spectral phenomenology. The calculation is based on an sp^3s^* model and on a surface Green-function matching analysis, partly using formalism previously developed and partly based on further formal developments presented and used here.

I. INTRODUCTION

The advances in modern growth techniques with good control of epitaxial crystal structures have caused a considerable interest in new varieties of artificially synthesized semiconductor materials.[1] In particular, GaAs/AlAs superlattices have received considerable attention as prototypes of artificial heterostructures combining alternate slabs of a direct-gap material (GaAs) and an indirect-gap one (AlAs), which results in novel electronic features such as band mixing or spatial confinement. These have been extensively studied by means of optical and/or electrical measurements[2–10] as well as in numerous calculations with varying degrees of sophistication.[11,12] Kronig-Penney or envelope-function models have been often used since their early introduction in this problem.[11] However, recent experiments with short-period superlattices in which at least one of the constituent slabs is less than 30 Å thick[7–10] indicate that their electronic properties cannot be sufficiently well described in terms of a single-band effective-mass theory and more elaborate models of the constituents as three-dimensional crystals are needed.

We shall study (001) superlattices and use the term *layer* meaning a *principal* layer consisting of *two atomic* layers, i.e., Al and As or Ga and As. The number of AlAs layers will be denoted as n and that of GaAs as m, while SL will denote a superlattice. Although these SL's have received considerable experimental and theoretical attention, two important issues still require further discussion, namely, the direct or indirect nature of the gap of short period SL's and the possible relationship between their electronic properties and those of ternary alloys with the corresponding concentrations. In fact, there is a substantial lack of agreement on both these questions. For instance, tight-binding,[13–15] pseudopotential[16] and first-principles self-consistent calculations[17] predict direct-gap materials for $n=m$ with $n \geq 2$, although they differ on the degree of hybridization of the lowest conduction band, and therefore on the preferential confinement of the band-edge states in either of the constituent slabs. A different picture was obtained from an empirical pseudopotential calculation,[18] where it was concluded that for $(n+m)<8$ the conduction-band-edge wave functions do not show any confinement and the short period SL's have direct or indirect gap according to the direct or indirect character of the corresponding alloys. A more recent tight-binding study[19] presents an intermediate picture with three regions in an (n,m) chart. (1) For $m \geq 10$ and irrespective of n, the lowest conduction-band state is associated with the GaAs Γ state (direct gap). (2) For $m < 10$ and $m \leq n$ it is assigned AlAs X character and it is concluded that electrons and holes are then separately confined in both real and momentum spaces. (3) There is an intermediate region, with $m > n$ and both n and $m < 10$, where the SL is claimed to have alloylike behavior. A similar situation prevails on the experimental side. While some authors claim that for $n > 2$ the SL's have direct energy gap,[9] others predict indirect gap for particular values of n and m.[7] More recently,[10] SL's where electrons and holes are separated in both real and momentum space have been reported for $(n,m)=(8,10)$, (19,19), and (31,29).

It should be noted that different calculations used different input parameters chosen to give different band offsets, when the crossing of zone-center- and zone-edge-related states is expected to be very sensitive to the relative alignment of the AlAs and GaAs band structures,[16] whence the direct or indirect character of the gap should also depend strongly on the band offset. This might explain some of the scatter found among the theoretical results. On the other hand, it is rather difficult experimentally not only to determine precisely the thickness of the SL period but also to assign direct or indirect character to an optical transition. For instance, scattering by disorder has been invoked to explain the comparable luminescence efficiency of direct- and indirect-gap samples.[10]

Most electronic and optical properties of semiconductor SL's, both theoretically and experimentally, tend to be discussed in terms of $\mathbf{k}$ states of the constituent bulk semiconductors. However, folding and remapping make the Brillouin zone of the SL different, and it is in terms of this new Brillouin zone that the electronic and optical properties of the SL must be discussed. Momentum for-

bidden transitions in an extended-zone scheme may become direct transitions in the reduced-zone scheme of the SL. On the other hand, most of the studies, either theoretical or experimental, are restricted to particular sets of values of (n,m), which are insufficient to obtain an overall view and to establish general trends.

The purpose of this paper is to study these issues with a sufficiently broad range of values of (n,m) and sufficiently detailed questions to obtain an overview from which some general pattern may emerge. Our approach is to study the SL material as a whole and to discuss the electronic properties in terms of the Brillouin zone of the SL. Special emphasis will be given not only to energy levels and dispersion relations but also to the local density of states associated with different SL states. The local projection of their spectral strength on all atomic layers of the SL period gives a direct picture of the spatial confinement in real space and this will be here studied in some detail.

The calculations will be based on sp^3s^* empirical tight-binding models, which give a good account of the respective bulk band structures, and on the surface Green-function matching (SGFM) method.

II. THEORY: SGFM ANALYSIS OF THE SUPERLATTICE

The general formal theory for discrete superlattices has been given elsewhere.[24,25] Here we summarize the main formulas, with emphasis on the practical aspects of the method for actual calculations. We also present some further formal theory which proves very useful in practice to calculate local densities of states. Geometry and notation are shown in Fig. 1. As in previous applications of this method[26–28] we shall employ the concept of *principal layer,* which is defined so that it interacts only with nearest-neighbor principal layers, and this accounts for all interactions in the crystal. The principal layer may contain one or more atomic layers, depending on the geometry and on the range of the interactions considered. After Fourier transform parallel to the interfaces, which

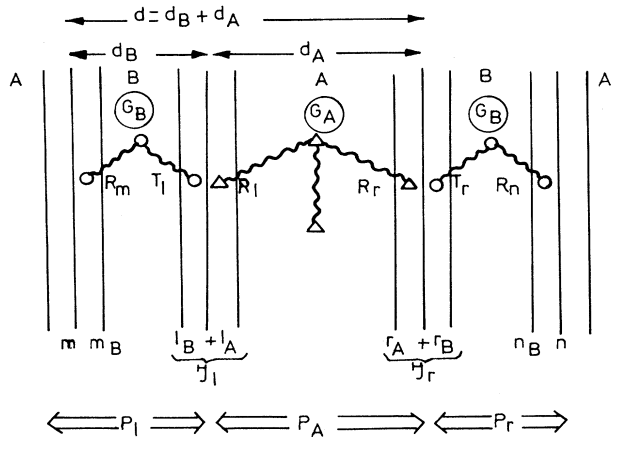

FIG. 1. Notation for the different projection domains in the superlattice. (See text).

introduces a two-dimensional crystal momentum κ, one atomic layer is described with as many basis states as are needed to describe the states of one atom. This determines the size of the diagonal term, a matrix in general, representing the local layer projection of, say, a Hamiltonian or Green-function matrix. In the following the term *layer* will indicate principal layer. Let N_M denote the number of layers of each material ($M=A,B$) and P_A the projector onto a slab of material A, bounded on the left (right) with B slabs having projectors P_l (P_r) (Fig. 1). The projector of the left boundary ($\mathcal{J}_l$) consists of a B part (l_B), contained in P_l, and an A part (l_A), contained in P_A. Likewise, the right boundary ($\mathcal{J}_r$) consists of (r_A), a part of P_A, and (r_B), a part of P_r. We concentrate initially on an A slab and take $\mathcal{J}=\mathcal{J}_l+\mathcal{J}_r$ as the unit of the entire interface projection domain. Projections and inverses are defined in their natural subdomains and then combined through the algebra in increasingly larger domains. For one interface each local projection yields matrices of a given size. Then through the coupling across the interface, these matrices are put together in a larger domain $\mathcal{J}_l=l_A+l_B$, thus obtaining supermatrices in (2×2) format. Finally, left and right are put together, through the propagation across the slabs, in a (4×4) supermatrix format, corresponding to $\mathcal{J}=\mathcal{J}_l+\mathcal{J}_r$. The size of this supermatrix is twice that corresponding to the (2×2) supermatrices integrated in it. The essence of the SGFM analysis is that all the matching features of the superlattice problem are included in this projection. This fixes the size of the superlattice secular matrix, irrespective of any increase in the size of the supercell. This is manifested only in the values of the cross elements of the corresponding Green functions, which contain all the propagating aspects of the superlattice problem. The superperiodicity is contained in the phase factor $f=\exp(iQd)$, where $d=d_A+d_B$. We now give the main SGFM formulas[24,25] to be used in the applications to follow.

Consider a homogeneous medium and start from the general definition

$$(EI-H)G=I\ , \tag{2.1}$$

H being a tight-binding Hamiltonian and I the complete unit of the space in which H and G are defined. In a superlattice I is the sum of alternate P_A and P_B projectors and H_s, with resolvent G_s, contains the corresponding $P_MH_MP_M$ terms and the cross terms embodying the A-B or B-A interactions across the interfaces. By definition of principal layer all these interactions are contained in the nondiagonal parts of subspaces like $\mathcal{J}_l$ or $\mathcal{J}_r$. Working now in the diagram of Fig. 1 we define

$$\hat{P}=P_l+P_r\ , \tag{2.2}$$

the sum of the two P_B projectors limiting P_A. Then all desired matrix elements of G_s can be obtained from

$$P_AG_sP_A = P_AG_AP_A+P_AG_A\tilde{G}_A^{-1}(\tilde{G}_{s,A}-\tilde{G}_A)\tilde{G}_A^{-1}G_AP_A\ , \tag{2.3a}$$

$$\hat{P}G_sP_A=\hat{P}G_B\hat{G}_B^{-1}\tilde{G}_{s,A}\tilde{G}_A^{-1}G_AP_A\ , \tag{2.3b}$$

where all the projections entering (2.3) have been defined elsewhere[24,25] and the (E,κ,f) dependence must be understood throughout.

The matching formula, yielding $\tilde{G}_{s,A}$, i.e., $\mathcal{J}G_s\mathcal{J}$, is

$$\tilde{G}_{s,A}^{-1}=\mathcal{J}E\mathcal{J}-\mathcal{J}H_s[\hat{P}G_B(f)\hat{G}_B^{-1}+P_AG_A\tilde{G}_A^{-1}]\ . \tag{2.4}$$

The spectral functions are calculated from the diagonal terms of G_s and the secular equation is given by

$$\det|\tilde{G}_{s,A}^{-1}|=0\ , \tag{2.5}$$

which yields the energy band structure $E(\kappa,Q)$ of the superlattice. The subscript A in $\tilde{G}_{s,A}$ is to remind us that we have chosen to project on the boundaries of an A slab. A complete set of dual formulas exists with the roles of A and B interchanged.

In order to perform real calculations one must obtain the Green-function elements entering the above formulas in a numerical way, for which it is essential to have a fast and reliable numerical algorithm. Here we use an iterative transfer-matrix algorithm[29] which has very fast convergence. Different transfer matrices can be defined for a given medium, namely,

$$\begin{aligned}
&G(n+1,n)=TG(n,n)\ ,\\
&G(n-1,n)=\bar{T}G(n,n)\ ,\\
&G(n,n+1)=G(n,n)S\ ,\\
&G(n,n-1)=G(n,n)\bar{S}\ .
\end{aligned} \tag{2.6}$$

These can all be calculated by the same iterative procedure. The SGFM formulas needed for actual calculations can then be cast in the following form:

$$\tilde{G}_{s,A}^{-1}=\begin{vmatrix}
l_B(E-H_s)l_B-l_BD_Bl_B & -l_BH_il_A & 0 & -l_BD_Br_B\\
-l_AH_il_B & l_A(E-H_s)l_A-l_AD_Al_A & -l_AD_Ar_A & 0\\
0 & -r_AD_Al_A & r_A(E-H_s)r_A-r_AD_Ar_A & -r_AH_ir_B\\
-r_BD_Bl_B & 0 & -r_BH_ir_A & r_B(E-H_s)r_B-r_BD_Br_B
\end{vmatrix}\ , \tag{2.7}$$

where

$$\begin{vmatrix} H_A(1,2) & 0\\ 0 & H_A(2,1)\end{vmatrix}\rho_A\tau_A^{-1}\equiv\begin{vmatrix} l_AD_Al_A & l_AD_Ar_A\\ r_AD_Al_A & r_AD_Ar_A\end{vmatrix}\ , \tag{2.8a}$$

$$\begin{vmatrix} H_B(2,1) & 0\\ 0 & H_B(1,2)\end{vmatrix}\rho_B\tau_B^{-1}\equiv\begin{vmatrix} l_BD_Bl_B & l_BD_Br_B\\ r_BD_Bl_B & r_BD_Br_B\end{vmatrix}\ , \tag{2.8b}$$

$$\rho_A=\begin{vmatrix} T_A & \bar{T}_A^{(\nu_A-1)}\\ T_A^{(\nu_A-1)} & \bar{T}_A\end{vmatrix},\quad \tau_A=\begin{vmatrix} 1_A & \bar{T}_A^{\nu_A}\\ T_A^{\nu_A} & 1_A\end{vmatrix}\ , \tag{2.9a}$$

$$\rho_B=\begin{vmatrix} \bar{T}_B & f^{-1}T_B^{(\nu_B-1)}\\ f\bar{T}_B^{(\nu_B-1)} & T_B\end{vmatrix},\quad \tau_B=\begin{vmatrix} 1_B & f^{-1}T_B^{\nu_B}\\ f\bar{T}_B^{\nu_B} & 1_B\end{vmatrix}\ , \tag{2.9b}$$

$T_M,\bar{T}_M$ $(M=A,B)$ being the transfer matrices introduced in (2.6) for medium M.

The local spectral strength in the layer n_A is obtained from

$$G_s(n_A,n_A)=\mathcal{G}_A+(T_A^{(n_A-1)},\bar{T}_A^{(\nu_A+1-n_A)})\mu_A\begin{pmatrix} S_A^{(n_A-1)}\\ \bar{S}_A^{(\nu_A+1-n_A)}\end{pmatrix}\ , \tag{2.10}$$

$$\mathcal{J}_A\mu_A\mathcal{J}_A\equiv\mu_A=\tau_A^{-1}(\mathcal{J}_A\tilde{G}_{s,A}\mathcal{J}_A-\tilde{g}_A)\sigma_A^{-1}\ , \tag{2.11}$$

$$\tilde{g}_A=\begin{vmatrix}\mathcal{G}_A & 0\\ 0 & \mathcal{G}_A\end{vmatrix},\quad \mathcal{G}_A=G_A(n_A,n_A),\quad \sigma_A=\begin{vmatrix} 1_A & S_A^{\nu_A}\\ \bar{S}_A^{\nu_A} & 1_A\end{vmatrix}\ . \tag{2.12}$$

The labeling of the layers and the meaning of ν_A and ν_B are shown in Fig. 2. In order to obtain the local density of states for given κ we must integrate over Q, the perpendicular component of the wave vector. The above formulas cannot be literally applied to the particular case in which one of the slabs is reduced to just one layer. This is the situation for periodic intercalation compounds, but the same method can be readily adapted to this case.[28] Note that a principal layer may, and usually does, contain more than one atomic layer. The local density of states is obtained from the trace of $G_s(n,n)$ and this sums over the atomic layers forming the layer n. The separate contributions from each atomic layer yield the corresponding local spectral strengths.

Now having calculated the LDOS in the A layers, the question is how to do the same in the B layers. The straightforward way would seem to be to resort to the set of dual formulas, with A and B and their roles interchanged. This would be correct, but not very practical, as the projections are then not in the domain (l,r) but in, say, (r,n). $\tilde{G}_{s,B}$, for instance, is not the same matrix as $\tilde{G}_{s,A}$, although both yield the same secular determinant. A parallel calculation of the dual formulas requires a recalculation of secular matrix and Green-function elements which would seem somewhat redundant as all the physical information should be contained in the projection on (l,r). We shall now prove that an alternative formulation for the B part is possible, with considerable practical advantage concerning both memory requirements and computer time. For this it is necessary to again set up the SGFM analysis on a formal basis.

All the formulas derived so far have been obtained by considering the response of the superlattice system to a standard unit input acting at some point of an A slab *and by projecting on the boundaries* (l,r) *of* A. We now consider a unit input acting at some point of B, say P_l' [Fig. 3(a)] and express the matching *again at the boundaries* (l,r) *of* A. We can write down the form of the amplitude in P_l and P_A, take P_l to l_B and P_A to l_A, i.e., make B and A meet at the l interface and then take P_l' to l_B. In this process P_l' always stays in B material and in the P_l slab, whence the amplitudes everywhere in P_l and P_A retain the same form. With this we can effect the (l,l) part of the matching. But we cannot take P_A and P_l to r and, moreover we cannot take P_l' to r while keeping the input on the same side of the matching domain, i.e., keeping constant the form of the amplitudes. The points to note are as follows. (1) One side of the matching domain consists of P_A. The "other side" consists of the P_l and P_r. Thus, when the input point scans the other side it must

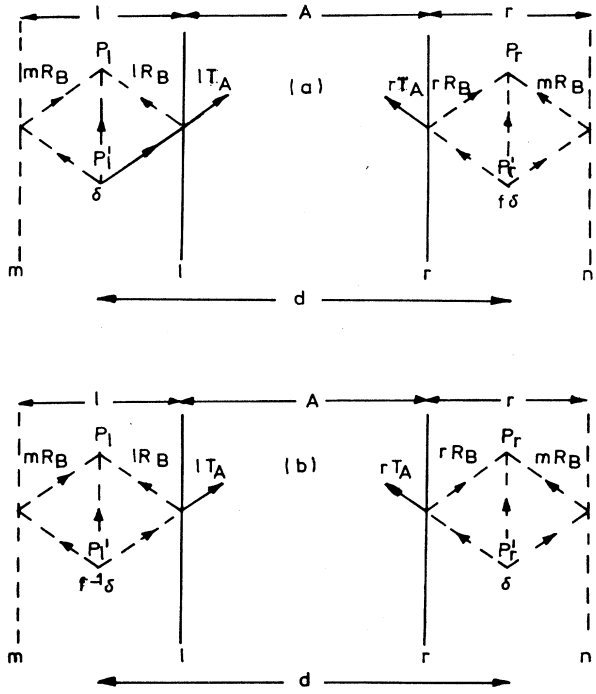

FIG. 3. The (matching) projection domain is chosen as $l+r$. A unit input outside the A layer requires another one with definite phase correlation at the point on the other side of A which is connected to the first one by a translation through $\pm d$.

scan *both* P_l *and* P_r. (ii) This is to be an eigenstate of a system having periodicity d, i.e., phase factor $f=\exp(iQd)$ and translations $\hat{t}$ through d. We must strictly keep this phase correspondence. Thus, for "matrix element" $P_jG_sP_l'$ $(j=l,A,r)$, we evaluate the amplitude at P_j when a standard unit input δ acts at P_l' and also an input $f\delta$ acts at $P_r'=\hat{t}P_l'$, as shown in Fig. 3(a).

We must now study

$$
\begin{aligned}
&P_lG_sP_l'=P_lG_BP_l'+P_lG_Bl\cdot lR_BP_l'+P_lG_Bm\cdot mR_BP_l' ,\\
&P_AG_sP_l'=P_AG_Al\cdot lT_AP_l'+P_AG_Ar\cdot rT_AP_l' , \qquad (2.13)\\
&P_rG_sP_l'=P_rG_B\hat{t}P_l'f+P_rG_Bn\cdot nR_BP_l'+P_rG_Br\cdot rR_BP_l' .
\end{aligned}
$$

We want to express this in terms of excitation of the matching domain $\mathcal{A}=l+r$, and then remission from it. By taking into account that $rG_BP_r'=mG_BP_l'$ and by following the procedure developed in Refs. 24 and 25 we obtain

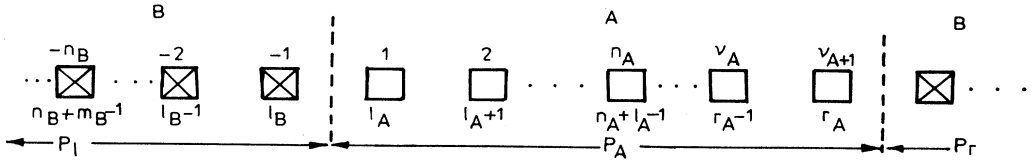

FIG. 2. Each square represents a principal layer. Shown are the labels used to denote them.

$$
\begin{aligned}
&P_l G_s P_l' = P_l G_B P_l' + P_L G_B l \cdot (R_{B,ll} \cdot l G_B P_l' + R_{B,lr} \cdot m G_B P_l' \cdot f) + f^{-1} P_l G_B m \cdot (R_{B,rl} \cdot l G_B P_l' + R_{B,rr} \cdot m G_B P_l' \cdot f) \ , \\
&P_A G_s P_l' = P_A G_A l \cdot (T_{A,ll} \cdot l G_B P_l' + T_{A,lr} \cdot m G_B P_l' \cdot f) + P_A G_A r \cdot (T_{A,rl} \cdot l G_B P_l' + T_{A,rr} \cdot m G_B P_l' \cdot f) \ , \\
&P_r G_s P_l' = P_r G_B \hat{t} P_l' \cdot f + f \cdot P_r G_B n \cdot (R_{B,ll} \cdot l G_B P_l' + R_{B,lr} \cdot m G_B P_l' \cdot f) + P_r G_B r \cdot (R_{B,rl} \cdot l G_B P_l' + R_{B,rr} \cdot m G_B P_l' \cdot f) \ .
\end{aligned} \tag{2.14}
$$

With this we have all the elements $P_j G_s P_l'$ $(j = l, A, r)$. Now we need $P_j G_s P_r'$. Then the standard input δ is at P_r' whereas we have an input $f^{-1}\delta$ at P_l' [Fig. 3(b)].

Now we must consider

$$
\begin{aligned}
&P_l G_s P_r' = P_l G_B \hat{t}^{-1} P_r' \cdot f^{-1} + P_l G_B l \cdot l R_B P_r' + P_l G_B m \cdot m R_B P_r' \ , \\
&P_A G_s P_r' = P_A G_A l \cdot l T_A P_r' + P_A G_A r \cdot r T_A P_r' \ , \\
&P_r G_s P_r' = P_r G_B P_r' + P_r G_B n \cdot n R_B P_r' + P_r G_B r \cdot r R_B P_r' \ .
\end{aligned} \tag{2.15}
$$

By taking into account that $m R_B P_r' = f^{-1} \cdot r R_B P_r'$, the above formulas are finally written in the form

$$
\begin{aligned}
&P_l G_s P_r' = P_l G_B \hat{t}^{-1} P_r' \cdot f^{-1} + P_l G_B l \cdot (R_{B,ll} \cdot n G_B P_r' \cdot f^{-1} + R_{B,lr} \cdot r G_B P_r') + f^{-1} P_l G_B m \cdot (R_{B,rl} \cdot n G_B P_r' \cdot f^{-1} + R_{B,rr} \cdot r G_B P_r') \ , \\
&P_A G_s P_r' = P_A G_A l \cdot (T_{A,ll} \cdot n G_B P_r' \cdot f^{-1} + T_{A,lr} \cdot r G_B P_r') + P_A G_A r \cdot (T_{A,rl} \cdot n G_B P_r' \cdot f^{-1} + T_{A,rr} \cdot r G_B P_r') \ , \\
&P_r G_s P_r' = P_r G_B P_r' + f \cdot P_r G_B n \cdot (R_{B,ll} \cdot n G_B P_r' \cdot f^{-1} + R_{B,lr} \cdot r G_B P_r') + P_r G_B r \cdot (R_{B,rl} \cdot n G_B P_r' \cdot f^{-1} + R_{B,rr} \cdot r G_B P_r') \ .
\end{aligned} \tag{2.16}
$$

We now define the following objects in the (2×2) supermatrix format with (l, r) labeling:

$$
\hat{P} G_B^{\phi} \mathcal{J} = \begin{vmatrix} P_l G_B l & f^{-1} P_l G_B m \\ f P_r G_B n & P_r G_B r \end{vmatrix} , \quad \mathcal{J} G_B^{\phi} \hat{P}' = \begin{vmatrix} l G_B P_l' & f^{-1} n G_B P_r' \\ f m G_B P_l' & r G_B P_r' \end{vmatrix} , \tag{2.17}
$$

$$
\mathcal{J} G_B^{\phi} \mathcal{J} = \begin{vmatrix} l G_B l & f^{-1} n G_B r \\ f n G_B l & r G_B r \end{vmatrix} , \quad \hat{P} G_B^{\phi} \hat{P}' = \begin{vmatrix} P_l G_B P_l' & f^{-1} P_l G_B \hat{t}^{-1} P_r' \\ f P_r G_B t P_l' & P_r G_B P_r' \end{vmatrix} . \tag{2.18}
$$

By using these expressions Eqs. (2.14) and (2.16) can be compacted into

$$
\hat{P} G_s \hat{P}' = \hat{P} G_B^{\phi} \hat{P}' + \hat{P} G_B^{\phi} \mathcal{J} \cdot R_B \cdot G_B^{\phi} \hat{P}' , \quad \hat{P}_A G_s \hat{P}' = P_A G_A \mathcal{J} \cdot T_A \cdot \mathcal{J} G_B^{\phi} \hat{P}' , \tag{2.19}
$$

R_B and T_A can be obtained by projecting (2.19) on the $\mathcal{J}$ domain. Then

$$
R_B = \hat{G}_B^{-1} (\tilde{G}_{s,A} - \hat{G}_B) \hat{G}_B^{-1} , \quad T_A = \tilde{G}_A^{-1} \tilde{G}_{s,A} \hat{G}_B^{-1} . \tag{2.20}
$$

Then the equations involving always projections on the domain (l, r) are written as

$$
\begin{aligned}
&P_A G_s P_A' = P_A G_A P_A' + P_A G_A \mathcal{J} \cdot \tilde{G}_A^{-1} (\tilde{G}_{s,A} - \tilde{G}_A) \tilde{G}_A^{-1} \cdot \mathcal{J} G_A P_A' \ , \\
&P_A G_s \hat{P}' = P_A G_A \mathcal{J} \cdot \tilde{G}_A^{-1} \tilde{G}_{s,A} \hat{G}_B^{-1} \cdot \mathcal{J} G_B^{\phi} \hat{P}' \ , \\
&\hat{P} G_s \hat{P}' = \hat{P} G_B^{\phi} \hat{P}' + \hat{P} G_B^{\phi} \mathcal{J} \cdot \hat{G}_B^{-1} (\tilde{G}_{s,A} - \hat{G}_B) \hat{G}_B^{-1} \cdot \mathcal{J} G_B^{\phi} \hat{P}' \ , \\
&\hat{P} G_s P_A' = \hat{P} G_B^{\phi} \mathcal{J} \cdot \hat{G}_B^{-1} \tilde{G}_{s,A} \tilde{G}_A^{-1} \cdot \mathcal{J} G_A P_A' \ .
\end{aligned} \tag{2.21}
$$

The local spectral strength in an n_B layer (Fig. 2) is then obtained

$$
G_s(n_B, n_B) = \mathcal{G}_B + (\bar{T}_B^{(n_B - 1)}, f^{-1} T_B^{(\nu_B + 1 - n_B)}) \mu_B \begin{bmatrix} \bar{S}_B^{(n_B - 1)} \\ f S_B^{(\nu_B + 1 - n_B)} \end{bmatrix} , \tag{2.22}
$$

$$
\mu_B = \tau_B^{-1} (\tilde{G}_{s,A} - \tilde{g}_B) \sigma_B^{-1} , \tag{2.23}
$$

$$
\tilde{g}_B = \begin{vmatrix} \mathcal{G}_B & 0 \\ 0 & \mathcal{G}_B \end{vmatrix} \sigma_B , \quad \mathcal{G}_B = G_B(n_B, n_A) , \quad \sigma_B = \begin{vmatrix} 1_B & f^{-1} \bar{S}_B^{\nu_B} \\ f S_B^{\nu_B} & 1_B \end{vmatrix} . \tag{2.24}
$$

Now the same scheme of calculation and the same projections are employed for the A and B parts of the superlattice in such a way that no redundant calculations must be performed.

The above formulas are prepared so that once the transfer matrices are evaluated by the iterative algorithm,[29] these are directly inserted in the algebra yielding the secular matrix and then the diagonal layer projections. Altogether, this provides a very efficient computational procedure.

III. RESULTS AND DISCUSSION

We have calculated the electronic properties of (001) AlAs/GaAs superlattices with n layers of AlAs and m of GaAs for $2 \leq n,m \leq 22$. One layer is 2.83 Å thick and contains two atomic layers, one of anions and one of cations. In the energy reference used here, E_v (AlAs) $=0$, E_c (AlAs)$=2.30$ eV, E_v (GaAs)$=0.55$ eV, and E_c (GaAs)$=2.10$ eV. The band offset is within experimentally accepted values. We have employed an sp^3s^* basis with the empirical tight-binding parameters of Vogl *et al.*[30]

A. Band-edge states

Figure 4 summarizes the overall picture. We refer always to the SL as a whole in every respect, including energy levels and momentum states. The top of the valence band (VB) is always at the Γ point and the corresponding wave function amplitude is always confined to the GaAs slabs, in agreement with all previous calculations. The bottom of the conduction band (CB) shows a variety of behaviors. Here we find *four* different regions. Region I: The gap is direct and the amplitude is confined to GaAs. This corresponds approximately to region I of (Ref. 19). It is customary to say here that in this region the conventional Kronig-Penney model is valid. However, we stress that this only holds for the band-edge-energy levels but nothing more, as will be seen later. Region II: The lowest CB state is confined to the AlAs slabs. In bulk AlAs crystal this would be an X state and the gap would be indirect, but we stress that in the SL the minimum E_c (SL) is at the Γ point of the SL and the gap is direct. Electrons and holes are separated in real space but the two band extrema have the same momentum in the reciprocal space of the SL. Region III: The boundaries of this region cannot always be precisely defined but the essence of it is that there is an intermediate zone between I and II where the SL has direct gap and the spectral strength of the bottom of the CB is distributed between the two constituents. So far these three regions are alike in that they all have direct gap but they differ in the spatial confinement of the states of the CB edge. Region IV: Here the bottom of the CB is at in-plane X points of the SL Brillouin zone, its amplitude is confined to the AlAs slabs and the gap is indirect. Electrons and holes are then separated in both real and momentum space. This region was also found in Ref. 19, although we find it for a much smaller range of values of (n,m). These are shown as dots in Fig. 4. The boundaries between zones can change by one or two layers within plausible limits, e.g., by taking a different value of the band offset within accepted experimental values, 0.4–0.56 eV. However, there is always a fourth intermediate zone, here labeled III, and this is significantly different from previous results. A more detailed characterization of this region, as well as an interpretation of region IV at variance with the proposed alloylike interpretation will be given below.

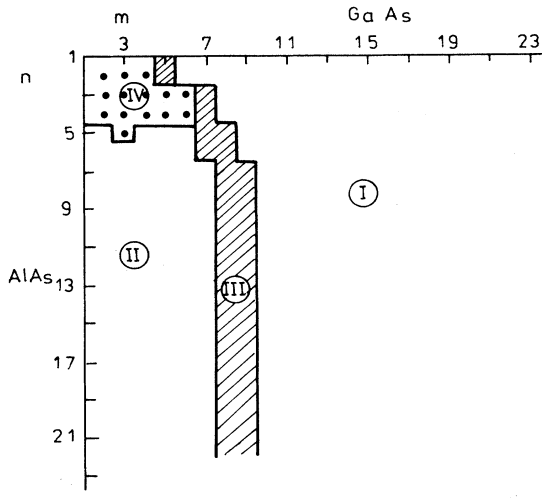

FIG. 4. The number of principal layers of AlAs-GaAs is n/m. A superlattice is a point in this chart. The four regions discussed in the text are shown here. The dots denote indirect gap SL's.

The energy levels E_c and E_v for the SL are given in Table I for $(5,5) \leq (n,m) \leq (12,12)$. The row $n=5$, $14 \leq m \leq 22$, and the columns $14 \leq n \leq 22$, $m=7$, and 10 in Fig. 4 are included in Table II. This extends the coverage of Fig. 4 in as much as is needed to cover all significant cases of regions I, II, and III. On moving along a row, e.g., $n=5$, m increasing, both E_c and E_v tend to the respective bulk values of GaAs crystal, but we shall see other electronic properties later which differ quite considerably. A different pattern is found on moving down a column, e.g., $m=10$. Then E_c, E_v, and E_g remain nearly constant. The same happens with column $m=7$, which is partly in region III and mostly in region II and, indeed, we have found the same for columns $m=8,9$, which are contained in region III. This approximate constancy does not depend on where the bottom of the CB of the SL is confined. Region IV is detailed in Table III, with $(2,2) \leq (n,m) \leq (4,7)$. Here the lowest-energy level for the Γ point of the SL raises above that for in plane X points and the gap is indirect.

Figure 5 gives the spatial distribution of the spectral strength for the band-edge states of some representative SL's corresponding to types I, II, and III. This has been calculated from the diagonal projections (2.10) and (2.22) of the composite Green function for each SL, extracting in each case the partial contribution giving the local spectral strength for the anion and cation atomic layers contained in each principal layer labeled n_A or n_B. In each case two separate curves run through the alternative local values for the anion (cation) atomic layers giving the dis-

TABLE I. Each (n,m) entry gives the corresponding values of E_c, E_v, and E_g, from top to bottom. (n,m) ranging from (5,5) to (12,12). An asterisk (plus) indicates that the corresponding state is confined to AlAs (GaAs). Absence of an asterisk or a plus indicates type III (see text).

		$m \rightarrow$GaAs							
		5	6	7	8	9	10	11	12
n	5	2.297*	2.296*	2.294	2.28	2.26$^+$	2.24$^+$	2.23$^+$	2.21$^+$
AlAs		0.40	0.43	0.45	0.46	0.48	0.49	0.50	0.50
		1.897	1.866	1.844	1.82	1.78	1.75	1.73	1.71
	6	2.29*	2.29*	2.29	2.28	2.26$^+$	2.25$^+$	2.23$^+$	2.22$^+$
		0.39	0.42	0.45	0.46	0.48	0.49	0.49	0.50
		1.90	1.87	1.84	1.82	1.78	1.76	1.74	1.72
	7	2.29*	2.29*	2.29*	2.28	2.27	2.25$^+$	2.23$^+$	2.22$^+$
		0.39	0.44	0.44	0.46	0.48	0.49	0.49	0.50
		1.90	1.87	1.85	1.82	1.79	1.76	1.74	1.72
	8	2.30*	2.29*	2.29*	2.28	2.27	2.25$^+$	2.23$^+$	2.22$^+$
		0.39	0.42	0.44	0.46	0.48	0.49	0.49	0.50
		1.91	1.87	1.85	1.82	1.79	1.76	1.74	1.72
	9	2.30*	2.29*	2.29*	2.28	2.27	2.25$^+$	2.23$^+$	2.22$^+$
		0.39	0.42	0.44	0.46	0.48	0.49	0.49	0.50
		1.91	1.87	1.85	1.82	1.79	1.76	1.74	1.72
	10	2.29*	2.28*	2.28*	2.28	2.27	2.25$^+$	2.24$^+$	2.22$^+$
		0.39	0.42	0.44	0.46	0.48	0.49	0.49	0.50
		1.90	1.86	1.84	1.82	1.79	1.76	1.75	1.72
	11	2.28*	2.28*	2.28*	2.28	2.27	2.25$^+$	2.24$^+$	2.22$^+$
		0.39	0.42	0.44	0.46	0.48	0.49	0.49	0.50
		1.89	1.86	1.84	1.82	1.79	1.76	1.75	1.72
	12	2.28*	2.28*	2.28*	2.28	2.27	2.25$^+$	2.24$^+$	2.22$^+$
		0.39	0.42	0.44	0.46	0.48	0.49	0.49	0.50
		1.89	1.86	1.84	1.82	1.79	1.76	1.75	1.72

tribution of amplitude between the two species. As expected, the top of the VB is always confined to the GaAs slabs and the amplitude is predominantly in the anions. For the cases (5,14) and (10,14), type I, the bottom of the CB is confined also to GaAs and the amplitude is mainly in the cations. For the cases (5,4) and (10,4), type II, the bottom of the CB is confined to AlAs and the amplitude is somewhat larger in the cations but the difference is rather small. For the cases (5,7) and (10,9), type III, the amplitude for the states at the bottom of the CB is distributed between the two constituent slabs, with larger strength for the cations but the difference for the two species is smaller on the AlAs side. This is simply a diffuse intermediate region between I and II for which states of both types are nearly degenerate in energy. The calculation cannot resolve in energy the states confined to GaAs from those confined to AlAs and the picture gives all the spectral strength at energy E_c. It is clear that a greater energy resolution would also be experimentally unlikely. Thus in practice we have a hybrid type of material, with spectral strength everywhere and a direct-gap value intermediate between the bulk values of E_g (GaAs, direct) and E_v (AlAs, indirect).

Figure 6 gives the dispersion relation for the highest

TABLE II. Same as Table I for the row $n=5$, $14 \leq m \leq 22$, and for the columns $m=7$ and $m=10$, with $14 \leq n \leq 22$.

	$m \rightarrow$AsGa				
AsAl	14	16	18	20	22
$n=5$	2.19$^+$	2.18$^+$	2.17$^+$	2.16$^+$	2.15$^+$
	0.51$^+$	0.52$^+$	0.52$^+$	0.53$^+$	0.53$^+$
	1.68	1.66	1.65	1.63	1.62
	$n \rightarrow$AsAl				
GaAs	14	15	16	19	22
$m=7$	2.28*	2.28*	2.28*	2.27*	2.27*
	0.44$^+$	0.44$^+$	0.44$^+$	0.44$^+$	0.44$^+$
	1.84	1.84	1.84	1.83	1.83
$m=10$	2.25$^+$	2.25$^+$	2.25$^+$	2.25$^+$	2.25$^+$
	0.49$^+$	0.49$^+$	0.49$^+$	0.49$^+$	0.49$^+$
	1.76	1.76	1.76	1.76	1.76

TABLE III. Each (n,m) entry gives the corresponding values of (from top to bottom) CB energy level at Γ, CB energy level at the in-plane X point, top of VB (always at Γ), and E_g (asterisks and pluses as in Tables I and II). Dots represent indirect-gap SL.

		$m \rightarrow$GaAs					
		2	3	4	5	6	7
n	2	2.373*	2.370+	2.334+	2.295+	2.266+	2.243+
$\rightarrow$		2.30*	2.30*	2.30*	2.30*	2.30*	2.30*
AlAs		0.30+	0.37+	0.41+	0.44	0.44+	0.44+
		2.00●	1.93●	1.89●	1.86	1.83	1.80
	3	2.327*	2.336*	2.328*	2.325*	2.301+	2.275+
		2.30*	2.30*	2.30*	2.30*	2.30*	2.30*
		0.26+	0.33+	0.38+	0.41+	0.44+	0.46+
		2.04●	1.97●	1.92●	1.89●	1.86●	1.84
	4	2.316*	2.304+	2.309*	2.305*	2.302*	2.291*
		2.30*	2.30*	2.30*	2.30*	2.30*	2.30*
		0.24+	0.31+	0.37+	0.40	0.43+	0.45+
		2.06●	1.99●	1.93●	1.9●	1.87●	1.85

VB and lowest CB branches for three SL's representing I, II, and III. Energy is plotted versus momentum perpendicular (parallel) to the interfaces for $\Gamma Z(\Gamma X)$. In the first case, the bands are practically flat, corresponding to strong confinement. Note that this also happens for the (5,7) case, of type III. This is in line with the discussion of Figs. 5(e) and 5(f). The bottom of the CB for type III SL's is confined, but both types of confinement I and II appear at practically the same energy. In the second case, E versus in-plane momentum, the extrema E_c and

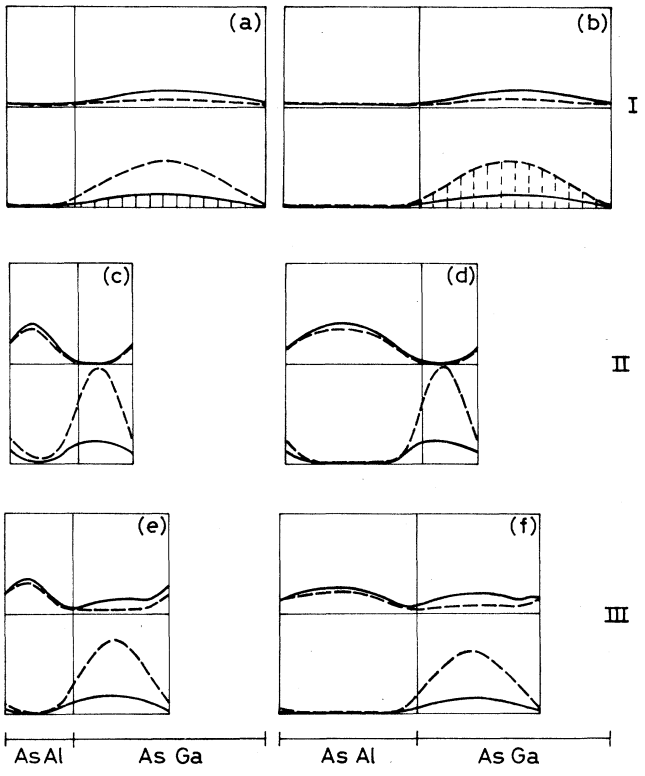

FIG. 5. Local spectral strength of some selected states at the Γ point of the SL for various values of (n,m). (a) and (b) correspond to (5,14) and (10,14) SL's, of type I; (c) and (d) to (5,4) and (10,4) SL's, of type II; (e) and (f) to (5,7) and (10,9) SL's, of type III. The figure displays the spatial distribution in the different atomic layers of the SL. A solid line represents cation layers and dashed line represents anion layers.

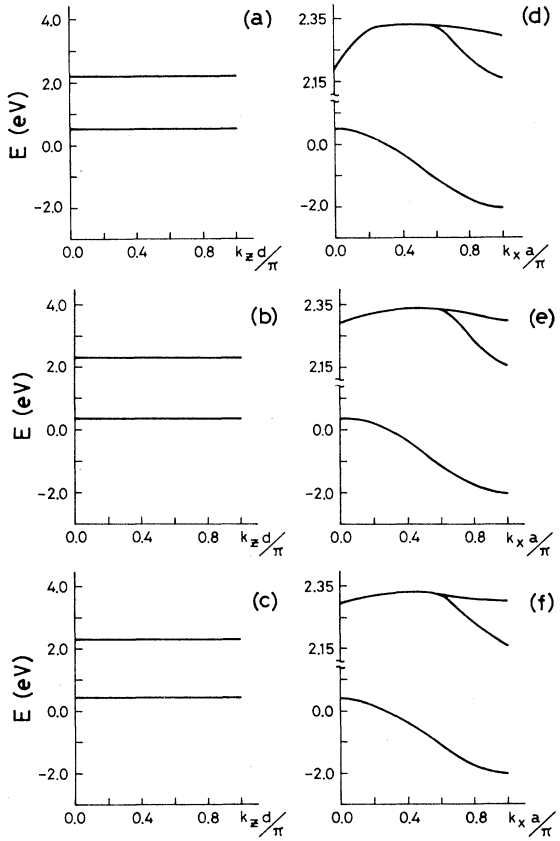

FIG. 6. Dispersion relation in the Γ-Z and Γ-X directions for the states at E_v and E_c. (a) and (d) correspond to the (5,14) SL of type I, (b) and (e) to (5,4) SL of type II, (c) and (f) to (5,7) SL of type III.

E_v appear at Γ and the VB branch is the more dispersive, qualitatively as in bulk GaAs states. Interface states appear in the gap away from Γ, e.g., for $\mathbf{k}=(0.6,0,0)\,\pi/a$ in Figs. 6(d)–6(f). Note also that although E_c tends monotonically to the bulk value E_c (GaAs) for increasing thickness, the energy level for the in plane X point of the SL stays at 2.3 eV, its bulk value for the AlAs crystal even for type I.

Similar dispersion curves are given in Fig. 7(b) for the indirect gap (3.3) SL, type IV, showing also the appearance of an interface state in the E versus in-plane momentum curve. The separate confinement of holes and electrons is seen in Fig. 7(a). For the latter we give the local amplitude for both the X ($E_v=2.3$ eV) and Γ ($E=2.336$) points. For these short period SL's even equal amounts of GaAs cannot compete with AlAs to attract electronic states at the bottom of the CB. These are all confined to the AlAs layers and the spectral strength at the anions is only slightly lower than at the cations, as in type II.

B. Short-period superlattices versus alloys

The substitutional ternary alloys $Al_xGa_{1-x}As$ are reasonably well described in terms of a virtual-crystal approximation because of the similar scattering properties of the Al and Ga potentials. The key electronic properties among them E_c, E_v, and hence E_g correspond to the weighted average of those for pure AlAs and GaAs. It has been suggested[18,19] that for small values of (n,m) the macroscopic composite SL should be rather similar to the ternary alloy with $x=n/(n+m)$. A detailed study of the present results does not support this view. Consider, for instance, the value of E_g. For the $x=0.5$ alloy this would be 1.39 eV. However, on moving along the diagonal $n=m$, the value of E_g starts *above* 1.99 eV and decreases steadily.

Moreover, the SL is an indirect-gap material only up to $n=5$ and then, for increasing n, it becomes a direct-gap material with $E_g<1.99$ eV, while the $x=0.5$ alloy has indirect gap, and crosses all the regions described above.

Furthermore, the SL's (2,3) and (4,6), for which $x=0.4$, have indirect gap, while the corresponding alloy has direct gap. We conclude that there are no grounds to view short-period AlAs-GaAs SL's as alloylike materials. The size of the constituent slabs is too small for any macroscopic feature to appear. The properties of the individual ionic layers tend to predominate, but the existence of a regular superperiodicity determines a type of materials for which the electronic structure must simply be calculated.

C. General behavior of the energy gap

The direct or indirect nature of the gap has already been discussed. Two plots of the value of E_g versus the length of the period are given in Fig. 8. Curve (a) corresponds to $n=m$, along the diagonal of Table I. The steady decrease of E_g is again at variance with the notion of alloylike behavior for short SL's. Existing experimental data show some scatter but follow the calculated curve rather well, with a general tendency towards the bulk value for GaAs. We note that this value is only approached for rather large values of $n=m$ of order 20, at least. The limit, of course, is at the GaAs value because

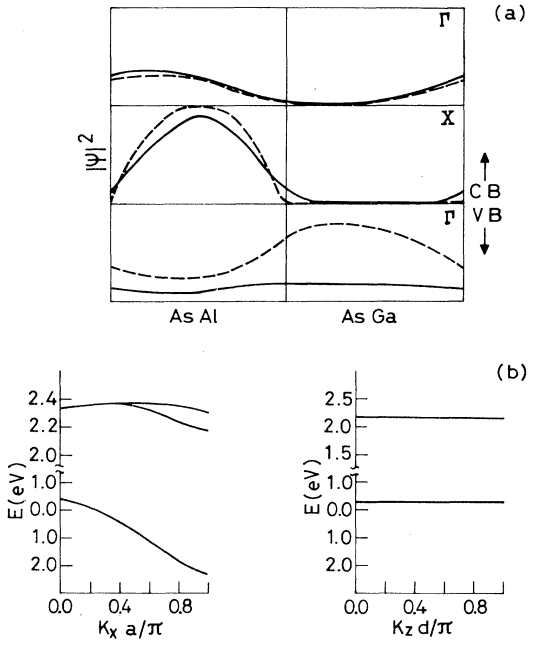

FIG. 7. (a) Same as Fig. 5, for the type IV SL (3,3). The state at E_v (0.332 eV) is at Γ and that at E_c (2.300 eV) is at the in-plane X point. Another state slightly above E_c ($E=2.336$) appearing at the Γ point is also displayed. (b) Dispersion relation for the band-edge states of the same SL.

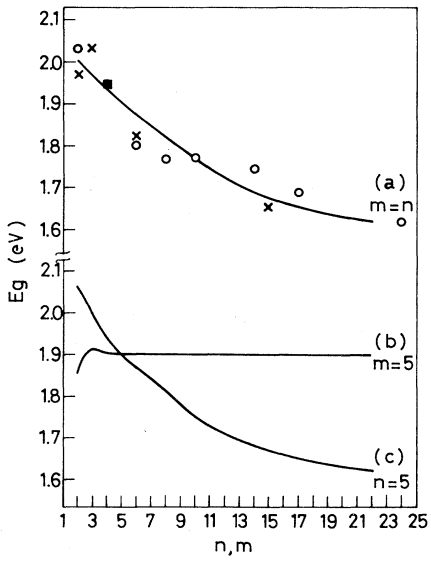

FIG. 8. Variation of the SL energy gap E_g with n and/or m is represented by a solid line which is calculated. Open circles and crosses are experimental for Refs. 9 and 7, respectively. (a) E_g vs $n=m$; (b) E_g vs n for fixed $m=5$. (c) E_g vs m for fixed $n=5$.

on moving along the diagonal $n=m$ we reach region I. The same tendency is observed for curve (c), which scans the row $n=5$ of Table I for increasing m. Curve (b) corresponds to the column $m=5$. For small n E_g increases at first and then tends to a constant value, as remarked above.

D. Electronic structure near the band edges

Folding effects accumulate states in a narrow energy interval, amounting in practice to degenerate states which may or may not be confined to the same constituent slabs. We have seen that this is the origin of region III [Figs. 4, 5 (e) and 5 (f)] which we have discussed by studying E_c. It is also interesting to study energies near the band edges. We shall take up the (5,5) and (5,14) SL's, as representatives of types II and I. Figures 9 and 10 give the local spectral strength for some selected states for given **k** points of the SL Brillouin zone.

Figure 9 corresponds to states near the band edges for the (5,5) SL. The spatial dependence of their amplitudes shows an interesting variety. The state at E_c has its strength in the AlAs slab as corresponds to type II. However, only slightly above E_c, the amplitude is nearly evenly shared and may even be larger in the GaAs slab, e.g., for $E=2.39$ eV. For the VB, we start from the spectral strength confined to GaAs and on moving slightly downwards in energy we find again a great variety. At $E=-0.03$, for instance, the amplitude tends to pile up near the interfaces and at $E=-0.19$ eV the amplitude is

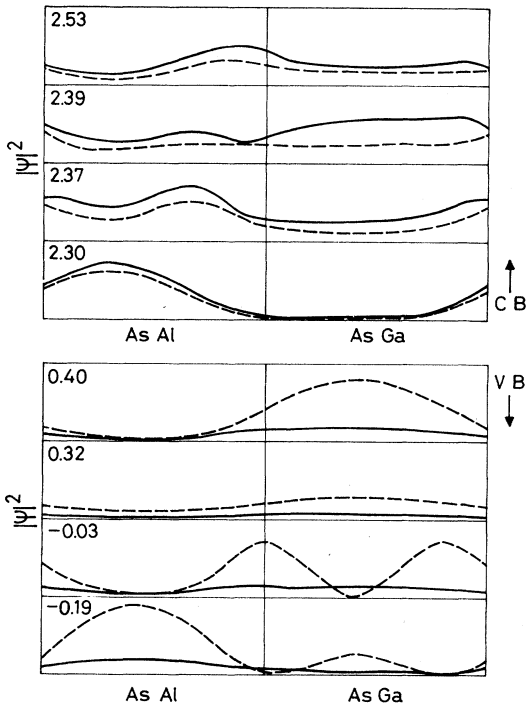

FIG. 9. (5,5) SL, type II. Local spectral strengths, as in Figs. 7 and 3, for four energy levels near E_v and four near E_c, as indicated.

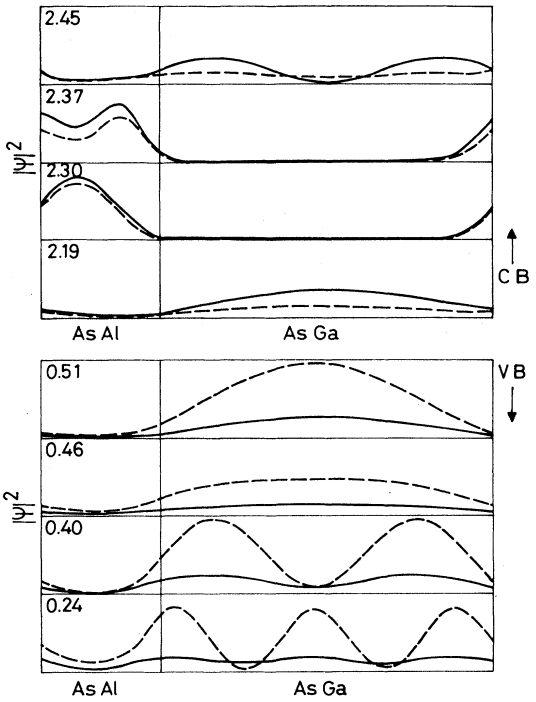

FIG. 10. Same as Fig. 9, for the (5,14) SL, type I.

mostly in AlAs.

The behavior found for the CB of a type-II SL has its counterpart in Fig. 10 for the (5,14) case, of type I. At E_c, the amplitude is confined to GaAs slightly above this energy there is predominant confinement to AlAs and then the amplitude returns to GaAs with oscillatory behavior. Starting from E_v downwards we find the amplitude confined to GaAs with increasingly fast oscillations.

Similar results are found in other cases. The spectral phenomenology of the SL's is greater than one might anticipate and the role of this in determining the various electronic properties of the material may constitute an interesting open problem. These properties are ultimately determined by the values of *both* n and m, not only by the SL period.

IV. FINAL COMMENTS

We have tried to produce a fairly comprehensive picture of (001) AlAs/GaAs superlattices within the frame of an sp^3s^* model. These SL's show a great variety of electronic structures. The top of the VB is always confined to the GaAs slabs but the bottom of the CB shows different behaviors. Folding effects cause the appearance of a region in the (n,m) chart, labeled as III in Fig. 4, where comparable amplitudes are found in both constituents. Altogether, we find *four* distinct types, only one having indirect gap in the Brillouin zone of the SL. We find no evidence anywhere of alloylike behavior. The SL is a distinct material in which the values of both n and m and the superperiodicity of the composite structure determine a great variety of behaviors. This concerns not only the band edges, but also the energy ranges near

them.

The SGFM formalism proves a practical method for doing the calculations for arbitrary values of n and m. Once the model has been specified the formulation is exact and any arbitrary increase in the size of the SL period can be handled with equal ease. The size of the matrices involved in the calculations remains strictly constant. In particular one can evaluate layer by layer the local amplitude or spectral strength of a given state of the SL. In this respect, the formal theory further developed in Sec. II is rather practical as it avoids having to evaluate the dual form of the secular matrix. The study of the energy ranges near the band edges reveals a rich variety which could not be surmised by simply studying the band edges. For instance, the (5,14) SL is definitely of type I. From the study of E_c and E_v only one would expect that the local electronic structure well inside the GaAs slabs is practically the same as in bulk GaAs. However the results (Fig. 10) show that it is very different indeed.

This diversity of the spectral phenomenology of the SL's is not a specific feature of the system studied here. Similar results are found for phonons in W-Mo super lattices.[31] This is rather a general consequence of the existence of superperiodicity. Various physical properties of the SL's, electronic, vibrational, electron-phonon interaction, etc., may depend on this. An interesting open problem lies ahead here.

ACKNOWLEDGMENT

This work was partially supported by the Dirección General de Investigación Cientifica y Técnica (Spanish Ministry of Education and Science), Grant No. 94-84.

[1]E.g., *Proceedings of the Seventh Molecular-Beam-Epitaxy Workshop, Cambridge, MA, 1986* [J. Vac. Sci. Tech. B **5**, 675 (1987)]; and *Proceedings of the Fourteenth International Symposium on Gallium Arsenide and Related Compounds,* edited by A. Christon and H. S. Rupprecht (IOP Conf. Ser. 91) (IOP, Bristol, 1988).

[2]M. Garriga, M. Cardona, N. E. Christensen, P. Lautenschlager, T. Isu, and K. Ploog, Phys. Rev. B **36**, 3254 (1987).

[3]M. Recio, J. L. Castaño, and F. Briones, Jpn. J. Appl. Phys. **27**, 1204 (1988).

[4]E. E. Mendez, E. Calleja, and W. I. Wang, Phys. Rev. B **34**, 6026 (1986).

[5]E. E. Mendez, W. I. Wang, E. Calleja, and T. Gonçalves da Silva, Appl. Phys. Lett. **50**, 1268 (1987).

[6]M. H. Meynadier, B. E. Nahory, J. H. Worlock, M. C. Tamargo, and J. L. de Miguel, Phys. Rev. Lett. **60**, 1338 (1988).

[7]D. S. Jiang, K. Kelting, T. Isu, H. J. Queisser, and K. Ploog, J. Appl. Phys. **63**, 845 (1988).

[8]G. Dahan, B. Etienne, F. Mollot, R. Planel, A. M. Jean-Louis, F. Alexandre, B. Jusserand, G. Le Roux, J. Y. Marzin, H. Savary, and B. Sermage, Phys. Rev. B **35**, 6207 (1987).

[9]A. Ishibashi, Y. Moni, M. Itabashi, and N. Watanabe, J. Appl. Phys. **58**, 2691 (1985).

[10]E. Finkman, H. D. Sturge, M. H. Meynhadier, R. E. Nahory, M. C. Tamargo, D. M. Hwang, and C. C. Chang, J. Lumin. **39**, 57 (1987).

[11]G. Bastard, Phys. Rev. B **25**, 7584 (1982).

[12]L. Brey and C. Tejedor, Phys. Rev. B **35**, 9112 (1987).

[13]J. N. Schulman and T. C. McGill, Phys. Rev. B **17**, 815 (1978).

[14]J. N. Schulman and Y. C. Chang, Phys. Rev. B **31**, 2056 (1985).

[15]S. Nara, Jpn. J. Appl. Phys. **26**, 690 (1987).

[16]M. A. Gell, D. Ninno, M. Jaros, and D. C. Herbert, Phys. Rev. B **34**, 2416 (1986).

[17]T. Nakayama and H. Kamimura, J. Phys. Soc. Jpn. **54**, 4726 (1985).

[18]W. Andreoni and R. Car, Phys. Rev. B **21**, 3334 (1980).

[19]J. Ihm, Appl. Phys. Lett. **50**, 1068 (1987).

[20]M. Cardona, T. Suemoto, N. E. Christensen, T. Isu, and K. Ploog, Phys. Rev. B **36**, 5906 (1987).

[21]N. E. Christensen, E. Molinari, and G. B. Bachelet, Solid State Commun. **56**, 125 (1985).

[22]S. Ciraci and I. P. Batra, Phys. Rev. B **36**, 1225 (1987).

[23]J. S. Nelson, C. Y. Fong, and I. P. Batra, Appl. Phys. Lett. **50**, 1595 (1987).

[24]F. Garcia-Moliner and V. R. Velasco, Phys. Scr. **34**, 252 (1986).

[25]F. Garcia-Moliner and V. R. Velasco, *Progress in Surface Science,* edited by S. G. Davidson (Academic, New York, 1986), Vol 21, p. 93.

[26]M. C. Muñoz, V. R. Velasco, and F. Garcia-Moliner, Phys. Scr. **35**, 504 (1987).

[27]M. C. Muñoz, V. R. Velasco, and F. Garcia-Moliner, *Progress in Surface Science,* edited by S. G. Davidson (Academic, New York, 1987), Vol. 26, p. 117.

[28]V. R. Velasco, F. Garcia-Moliner, L. Miglio, and L. Colombo, Phys. Rev. B **38**, 3172 (1988).

[29]M. P. López-Sancho, J. M. López-Sancho, and J. Rubio, J. Phys. F **14**, 1205 (1984); **15**, 851 (1985).

[30]P. Vogl, H. P. Hjalmarson, and J. D. Dow, J. Phys. Chem. Solids **44**, 365 (1983).

[31]R. Brito-Orta, V. R. Velasco, and F. Garcia-Moliner, Phys. Rev. B **38**, 9631 (1988).